Mars Without the Southern Perennial CO 2 Cover

E. Vos, O Aharonson, F. Forget

AGU ADVANCING EARTH AND SPACE SCIENCES

Geophysical Research Letters

RESEARCH LETTER
10.1029/2024GL113274

Mars Without the Southern Perennial CO_2 Cover

E. Vos[1,2], O. Aharonson[1,3], and F. Forget[2]

[1]Department of Earth and Planetary Sciences, Weizmann Institute of Science, Rehovot, Israel, [2]Laboratoire de Météorologie Dynamique/IPSL, Sorbonne Université, ENS,PSL Research University, Ecole Polytechnique, CNRS, Paris, France, [3]Planetary Science Institute, Tucson, AZ, USA

Key Points:

- We perform simulations using the Mars Planetary Climate Model in the absenceof the southern perennial CO_2 cover
- The atmospheric humidity in the southern hemisphere polar region is more than doubled for an albedo decrease of 15%
- Exposing some of the South Polar Layered Deposits (SPLD) basal unit ice makes the SPLD become the dominantsource of atmospheric humidity

Supporting Information:

Supporting Information may be found in the online version of this article.

Correspondence to:

E. Vos,
eran.vos@lmd.ipsl.fr

Citation:

Vos, E., Aharonson, O., & Forget, F. (2025). Mars without the southern perennial CO_2 cover. *Geophysical Research Letters*, *52*, e2024GL113274. https://doi.org/10.1029/2024GL113274

Received 23 OCT 2024
Accepted 5 JAN 2025

Abstract The Martian South Polar Layered Deposits (SPLD) are composed mostly of ice and dust with a thin perennial CO_2 cover and some internal CO_2 ice layers. In the North, the seasonal CO_2 cap is lost during summer, allowing H_2O ice to sublimate into the atmosphere. In the South, the perennial CO_2 cover prevents H_2O ice sublimation. This work uses the Mars Planetary Climate Model to investigate how the H_2O and CO_2 cycles are affected if the thin perennial CO_2 SPLD cover is lost. We find that during southern summer, the atmospheric water content will more than double in the south polar region. However, on a global scale, the NPLD is still the dominant source of humidity because of its larger surface area. When exposing some of the South Polar Cap buried water ice, the south polar cap becomes the dominant source of atmospheric humidity due to Mars's spin-orbital alignment.

Plain Language Summary Water and carbon dioxide ice on Mars are abundant in the polar caps. The south polar cap is composed of water ice and dust with some buried layers of carbon dioxide ice. At the cap top is a perennial thin cover of carbon dioxide ice that pins the surface temperature to 145 K and prevents water ice from sublimating. This work uses a Martian global climate model to test how the loss of the southern polar cap's perennial carbon dioxide ice cover affects the atmospheric humidity. We find that the atmospheric water content in the south polar region will more than double during southern summer. However, on a global scale, The NPLD is still the dominant source of atmospheric humidity because of the much larger surface area.

1. Introduction

The Martian Polar Layered Deposits (PLDs) are layered polar caps that are suggested to be mostly composed of dust and water ice, while the atmosphere is primarily composed of CO_2. During the winter, some of the atmospheric CO_2 condenses to form a seasonal cap that sublimates during the summer, strongly affecting the seasonal surface pressure. In the South Pole, CO_2 can also be found as layers in the SPLD (Phillips et al., 2011) and as a thin perennial cover that survives the summer (Byrne, 2009). There are observations of morphological changes in the South Polar Cap thin perennial CO_2 cover in the last few decades (Byrne, 2009; Malin et al., 2001; Thomas et al., 2016, 2020). Previous work suggested that, at present, the perennial South Polar Cap CO_2 cover is slowly decreasing and will be lost in several decades (Thomas et al., 2005). However, more recent observations suggest that it is difficult to determine the present mass balance of the perennial South Polar Cap CO_2 cover (Lange et al., 2022; Piqueux & Christensen, 2008), primarily because of the complexity in separating the vertical mass balance from the horizontal one (Thomas et al., 2016). Previous modeling suggests that the buried CO_2 might buffer the CO_2 cover over long timescales (P. Buhler et al., 2020). However, the thin perennial CO_2 cover appears to be only marginally stable at present and may be easily lost upon small perturbations of climatic conditions on short timescales (P. B. Buhler & Piqueux, 2021).

Water ice can be found in several forms on Mars, primarily in the PLDs (Byrne, 2009), in the mid-latitude subsurface (Dundas et al., 2023; Mellon et al., 2009; Morgan et al., 2021; Smith et al., 2009), and in winter seasonal frost. Observations from Viking (Haberle & Jakosky, 1990) and the Thermal Emission Spectrometer (TES) (M. D. Smith, 2004) of atmospheric water vapor show that the northern summer is more humid than the southern summer.

The global average atmospheric humidity is 7.3 pr. μm, with a peak value of ~70 pr. μm in summertime over the NPLD exposed water ice (M. D. Smith, 2004). In the south, summer humidity over the ice cap peaks at only ~25 pr. μm in the recent ~15 Mars Years in the TES data set (M. D. Smith, 2004). Older measurements from ground-based telescopes and the Viking Orbiters indicate higher, ~50 pr. μm, south polar summertime humidity (Jakosky

& Barker, 1984) but modern reanalysis of those data suggests atmospheric humidity could have been lower (Fedorova et al., 2010).

Innanen et al. (2022) calculated the amount of water vapor sourced from the South Polar Cap so-called Swiss-Cheese Terrain and found that it is negligible. However, based on extrapolation, they suggest that if all of the South Polar Residual Cap (SPRC) were lost, it could be enough to reproduce the high humidity measured by Viking and ground-based telescopes. The North Polar Cap albedo is lower than terrestrial polar ice because of dust contamination or large ice grains (Byrne, 2009; Byrne et al., 2008). The South Polar Cap albedo is higher than the NPLD because of the perennial CO_2 cover. However, in some high-resolution photos, steep-sided SPRC CO_2 pits ablate, and low-slope margins of the SPRC CO_2 grow, with typically a net increase in dark water ice exposure (P. B. Buhler et al., 2017; Thomas et al., 2016). Models suggest that during global dust storm years, the sublimation of the dark locations in the SPLD is enhanced (Bonev et al., 2008). Decreasing the surface albedo can cause positive feedback by lifting more dust particles via increased wind stresses or by a more unstable atmosphere (Fenton et al., 2007). The surface area of the SPLD is much smaller than the NPLD (Byrne, 2009; Zuber et al., 1998). Yet, past studies showed that the basal unit of the South Polar Cap that contains water ice beneath a dust covered layer is shallower and more extensive than the equivalent unit in the north, in some places extending to latitude 75°S (Plaut et al., 2007). Using a GCM, Montmessin et al. (2007) calculated the loss of water ice at the South Pole for the case ice is extended from the pole to latitude 80°S. They suggest the loss rate can reach more than 1 mm per Mars Year. However, in their model, the clouds do not interact with the radiation, which has been shown to be important for a humid atmosphere (Madeleine et al., 2012).

The CO_2 and H_2O cycles affect each other in various ways. Condensation and sublimation of CO_2 frost alter the albedo, modifying the surface temperature. The presence of CO_2 also pins the surface temperature to the frost point, providing a stable cold-trap for water. The CO_2 atmospheric cycle changes the surface pressure and, therefore, the frost-point temperature. H_2O ice can act as cloud condensation nuclei for CO_2 clouds (Alsaeed & Hayne, 2022). Therefore, understanding the CO_2 and H_2O cycles on Mars is fundamental for understanding present, past, and future climate, as well as for future human exploration. This work uses a Martian Planetary Climate Model (PCM) (Forget et al., 1999) formally known as the Laboratoire de Météorologie Dynamique Mars Global Climate Model to test how exposing water ice in the South Pole will affect the CO_2 and water cycles.

We use the Mars PCM with the complete water cycle that includes treatment of surface ice, atmospheric vapor, and water ice cloud microphysics up to 100 km and has been described in detail previously (Forget et al., 1999, 2011; Madeleine et al., 2009, 2011; Navarro et al., 2014). In this model, the dust and the water ice clouds are radiatively active (Madeleine et al., 2011, 2012; Navarro et al., 2014). The model simulates important physical processes in the Martian atmosphere, such as turbulence mixing, cloud condensation, ice sedimentation, and gravity waves, as described in the cited papers. Surface-atmosphere interactions such as CO_2 and water sublimation are also included in the PCM. The PCM resolution is 64 longitudes $\times$ 49 latitudes $\times$ 32 vertical layers with increasing thickness with height. The dust opacity profile is set to the mean of observations suggested to best represent Mars (Montabone et al., 2015). The surface ice distribution is similar to present-day distribution except for the last test, where we mirror the north-polar region surface ice to the south, as explained in the text. The surface properties such as thermal inertia and emissivity are set to the annual mean values based on measurements from the Mars Global Surveyor TES (Putzig et al., 2005). However, the surface albedo changes both in space and time, especially in the polar regions. In the model, we set the value to the broadband albedo measured by the TES solar channel (as a function of time) multiplied by a constant value to account for the non-Lambertian behavior of ice and atmospheric dust (the bond albedo is larger than the reflectance from space at nadir through a dusty atmosphere) (Forget et al., 2011; Vincendon et al., 2015). For the reference run here, this factor, defined as $f_{SA} = A_{\mathrm{bond}}/A_{\mathrm{obs}}$, is set to 1.6. For runs where we reduce the South Polar Cap albedo so that the CO_2 perennial cap is lost during southern summer, the southern albedo factor f_{SA} is reduced as specified below. The low albedo can be caused by extra surface dust loading or a volcanic eruption that injects dark particles into the atmosphere. The choice of all other model parameters, such as ice albedo, subsurface thermal inertia, and more, is identical to that published in Vos et al. (2022) and previous works except for clouds, which in this work are radiatively active. A list of key parameter values is also provided in the Supporting Information S1.

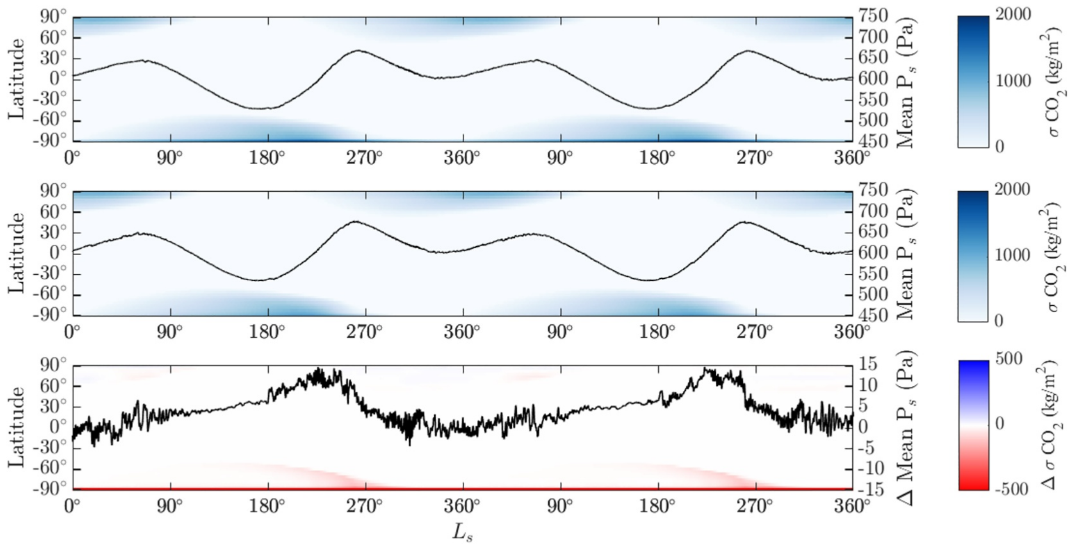

Figure 1. Zonal mean surface CO_2 ice column density (colors) and surface pressure (black line) compared between the reference run ($f_{SA} = 1.6$) and a lower southern polar albedo ($f_{SA} = 1.35$) run. σ stands for CO_2 surface density, and Δ for the difference between the two cases. The top panel is the reference case, the middle panel is the decreased albedo case, and the bottom panel is the difference between the runs (decreased albedo case minus the reference). For the lower South Polar albedo case, the southern perennial CO_2 cover is completely lost during southern summer, and there is a corresponding increase in surface pressure.

2. Results

We use the Mars PCM to study the differences in the water and CO_2 cycles in different cases. We begin by comparing two cases. The first is current Mars, which may be considered the reference case. This model matches many others used in other works (Madeleine et al., 2014; Navarro et al., 2014; Vos et al., 2022; Vos, Aharonson, Schörghofer, Forget, Lange, & Millour, 2023; Vos, Aharonson, Schörghofer, Forget, & Millour, 2023), and has been calibrated to match observations (Forget et al., 2011; Millour et al., 2018). The second is the same model, but with an adjusted South Polar Cap albedo such that the thin perennial CO_2 cap is lost during southern summer. (This can be seen in Figure SM1 where we plot the surface CO_2 as a function of time for the southernmost point of our simulations where CO_2 survives the longest, for the reference and for the decreased albedo cases.)

In the figures below, we compare the various cases mentioned above. In Figure 1, we compare the reference case with $f_{SA} = 1.6$ with $f_{SA} = 1.35$, and show the zonal mean CO_2 surface ice for each case and the difference between them for years 5 and 6 after letting the model equilibrate for 4 years. In the reference run, during winter, the CO_2 seasonal cap builds and extends below latitude 50°, before being lost during the summer. In northern summer, the CO_2 cap is completely lost, while a small cap persists throughout the year in the southern hemisphere. When the South Polar Cap albedo is decreased by 15% ($f_{SA} = 1.35$), the perennial southern CO_2 cover is lost for several sols at $L_s \sim 297°$(Figure 1, Figure SM1). In addition to the loss of the perennial CO_2 cover, the retreat of the seasonal CO_2 ice cap begins earlier, as can be seen in the bottom panel of Figure 1 from latitude $\sim -60°$ to the pole. Additional simulations show that reducing the southern cap albedo even further enhances this effect.

Figure 1 also compares the reference case $f_{SA} = 1.6$ with $f_{SA} = 1.35$ in global mean surface pressure. We obtain the usual double-peak pressure curve for the reference case with an annual mean of $\sim$610 Pa. The peaks result from the minimum in the seasonal CO_2 caps, where the southern summer peak is larger. A similar behavior is seen when the Southern Cap albedo is decreased by 15% (middle panel). However, examining the difference between the cases, there is an increase of up to 15 Pa during southern summer due to the greater loss of the southern perennial CO_2 cap. In addition, smaller perturbations are seen, with differences of a few Pa, caused by smaller effects, such as instantaneous changes in local albedo due to the retreat of the seasonal cap that locally modifies the temperatures and winds but only slightly modifies the global pressure.

Figure 2 compares the reference case $f_{SA} = 1.6$ and $f_{SA} = 1.35$ for the zonal mean atmospheric water column. The top panel is the reference, the middle is for $f_{SA} = 1.35$, and the bottom is the difference between the cases. The top

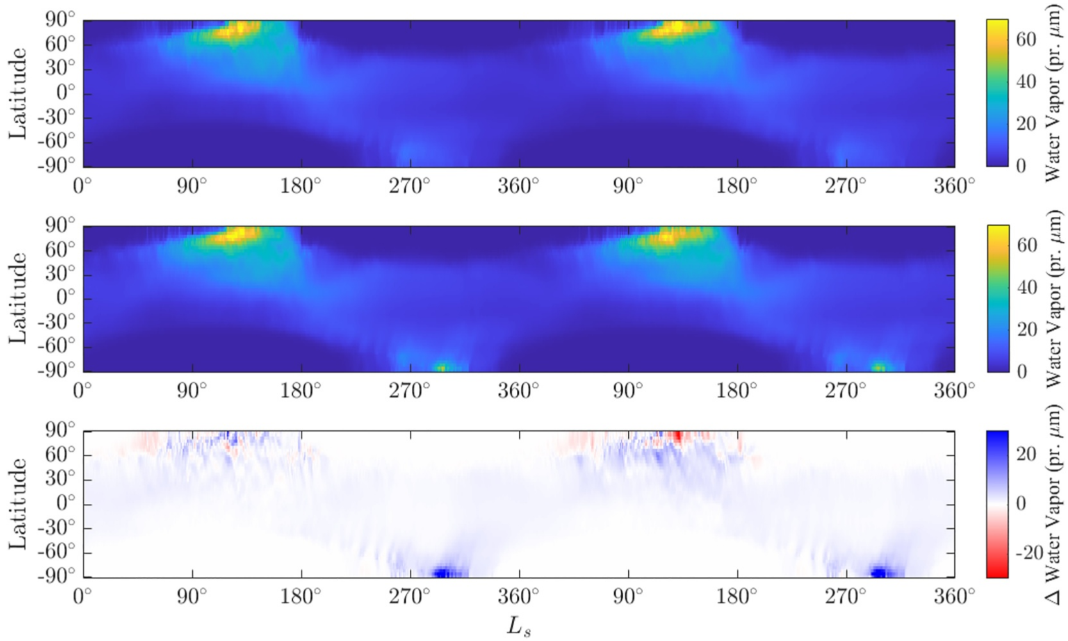

Figure 2. Same as Figure 1 but for the zonal mean atmospheric water content in column precipitable microns. For the lower Southern Polar albedo, the global atmospheric water content grows and more than doubles in the South Polar region.

panel shows the water vapor content in the atmosphere with a good match to TES data (M. D. Smith, 2004). During northern summer (L_s between 90 and 180°), the atmospheric water vapor column reaches 65–70 pr. μm close to the NPLD and decreases as it approaches the equator. During southern summer, the atmospheric water vapor column reaches 20 pr. μm in a small area. The frost point of CO_2 is ~145 K. Hence, the majority of the water ice cannot sublimate in the southern cap for the reference case because it is locked below the CO_2 ice. Once we decrease the southern cap f_{SA} to 1.35 (middle panel) and the CO_2 perennial ice is lost, the temperature can rise, and water ice is exposed to the atmosphere and can sublimate. In the northern hemisphere summer, we obtain similar results. However, in the southern hemisphere polar region, a larger amount of water enters the atmosphere and reaches 45–50 pr. μm. Looking at the difference between the two cases (bottom panel), we find that in the absence of the South Polar Cap CO_2 cover, the entire global atmospheric water content has moderately increased, and close to the South Polar Cap, the humidity has more than doubled. We plot 2 years here to show there is also interannual variability in the model, especially in the North Polar region during the northern summer. During this time, small perturbations are caused by changes in local albedo due to modifications in the seasonal cap retreat timing. These, in turn, modify the temperatures, affecting the local cloud coverage.

As previously mentioned, the South Polar Cap surface area is smaller than the North Polar Cap (Byrne, 2009; Zuber et al., 1998). However, mapping shows (Plaut et al., 2007) that the SPLD basal unit, which is interpreted to consist of water ice covered by dust is considerably more extensive than the SPLD (and is also larger than the NPLD); hence, exposing the SPLD basal unit would be expected to lead to a much larger effect on the atmospheric water content than the result shown in Figure 3. Note, the dust cover above the SPLD acts as a sublimation barrier. The lag layer needs to be removed (at least partially) to allow sublimation (?Bramson et al., 2019; Vos et al., 2019). To test this case, we enlarged the surface area of the exposed water ice in the South to mirror the surface area of the NPLD. This assumption is not intended to reflect specific conditions but rather is provided as an example designed to investigate the effect of exposing some of the SPLD basal unit with a given surface area to the atmosphere as may have been the case in the past (Emmett et al., 2020; Levrard et al., 2007; Vos et al., 2022). In addition, this test allows probing the humidity input variations caused by the asymmetry of the perihelion alignment. Although this experiment is artificial, it helps reveal the relationship between exposed ice surface area and the atmospheric water content.

Figure 3 summarizes the results of this test. We plot the global mean atmospheric water content as a function of the solar longitude (L_s) for five cases: the reference case with $f_{SA} = 1.6$ and with decreased southern albedo shown

10.1029/2024GL113274

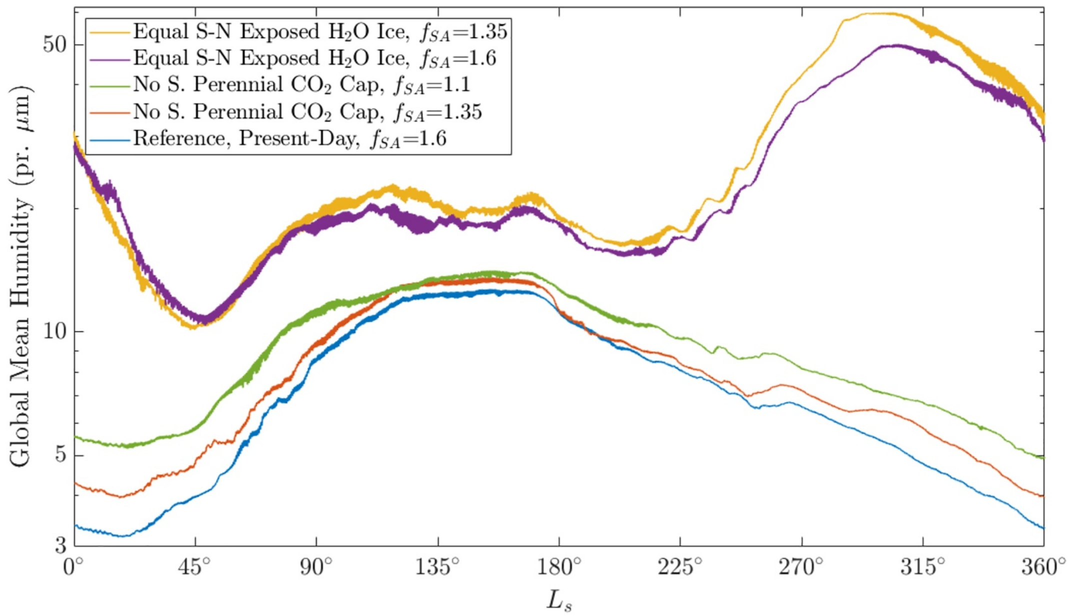

Figure 3. Global mean atmospheric water content in precipitable microns as a function L_s for the five cases: Reference, decrease southern albedo with a $f_{SA} = 1.35$, decrease southern albedo with a $f_{SA} = 1.1$, equal south and north water ice surface area with a $f_{SA} = 1.6$, and 1.35. Note the logarithmic vertical scale. For the lower southern cap albedo, the atmospheric water content during southern summer is larger. For the cases of equal north and south polar caps surface area, the atmospheric water content is an order of magnitude larger during southern summer.

in Figure 3 ($f_{SA} = 1.35$). In addition, we plot an even lower albedo case with $f_{SA} = 1.1$ and two cases with an equal surface area of water ice exposed in both poles with a f_{SA} of 1.6 and 1.35. The diurnal cycles act to add fluctuations of up to 5.5 pr. μm. The additional non-monotonic perturbations are due to instantaneous changes in albedo caused by a shift in the seasonal cap margin or the cloud distribution and size, which, in turn, change the energy balance and affect the temperatures. These temperature modifications change the atmospheric water capacity, again affecting the ice cloud distribution. For the three cases with present-day water ice surface area of the present-day extent of the residual ice caps, we observe the same trend, a maximum during northern summer with a global mean humidity of ~13 pr. μm and a decrease in the atmospheric water content as southern summer approaches. For the 15% lower albedo case ($f_{SA} = 1.35$), the perennial CO_2 cover is lost during the summer, and there is a 15% and 30% increase in the global mean atmospheric water content during northern and southern summer, respectively. We also plot the lowest albedo case ($f_{SA} = 1.1$) to show that decreasing the albedo further allows more ice to sublimate during southern summer. In addition to the three cases discussed above, we consider two cases with an increased southern cap surface area to match the size of the North Polar Cap exposed ice, with the same albedo values mentioned above ($f_{SA} = 1.6$, 1.35). For these cases, there is a large increase in the global atmospheric water vapor content of up to 11 times during southern summer compared to the reference case. The diurnal changes are also larger, because more ice condenses during the night. Note that in these cases, the maximum global mean water content now occurs in southern summer instead of northern summer. When comparing the two cases with the larger water ice surface area in the south, naturally, less surface ice sublimates for the higher southern albedo, and hence, the atmosphere is less humid during southern summer. This highlights the large north-south asymmetry in maximum insolation caused by the perihelion alignment and consequent water ice sublimation, also shown in previous work (Levrard et al., 2007; Montmessin et al., 2007; Vos, Aharonson, Schörghofer, Forget, Lange, & Millour, 2023; Vos, Aharonson, Schörghofer, Forget, & Millour, 2023).

3. Summary and Discussion

In this work, we use the Mars PCM to test how the H_2O and CO_2 cycles would be affected by exposing surface ice in the south polar region by either reducing the south perennial CO_2 albedo or by removing the lag covering some of the SPLD basal unit.

This experiment helps reveal the relationship between the exposure of South Polar Cap ice and the global water cycle. Note that while the precise configuration needed for loss of the CO_2 perennial cover can change with model parameters, the effect of exposing ice on the water cycle remains robust.

In our simulations, reducing the South Polar Cap albedo by 15% is sufficient to result in a loss of the South Polar Cap perennial CO_2 cover for several sols at the end of southern summer. The removal of the perennial CO_2 is naturally accompanied by an increase in atmospheric pressure during southern summer. Although the CO_2 perennial ice was lost over a small surface area, the effect on the H_2O cycle is significant. The global humidity increases by ~30%, and more than doubles in the south polar region. Decreasing the South Polar Cap albedo further allows more ice to sublimate and amplifies the atmospheric vapor content (Figure 3). Differences in temperature and clouds also cause smaller perturbations. Our results are in agreement with Innanen et al. (2022), who calculated the ice loss from the South Polar Swiss Cheese Terrain and then extrapolated to get the ice loss from the entire SPRC.

Observations show that the SPLD basal unit, which contains a large fraction of water ice beneath a dusty lag layer, is much larger in surface area (more than an order of magnitude) than the perennial CO_2 ice cover (Plaut et al., 2007). We also tested two cases of a larger exposed water ice surface area in the south-polar region equal to the NPLD size. In these cases, the atmospheric water content is much larger, up to an order of magnitude larger during southern summer. Moreover, the southern summer is more humid than the northern summer, unlike at present. This large difference is caused by the perihelion alignment combined with the present-day high eccentricity, which leads to shorter and more intense summers in the southern hemisphere (Vos, Aharonson, Schörghofer, Forget, Lange, & Millour, 2023; Vos, Aharonson, Schörghofer, Forget, & Millour, 2023). For example, the mean summer daily insolation is approximately 40% higher at latitude 80°S than at 80°N (Van Hemelrijck, 1983). Note that both caps are stable in this scenario. However, changing parameters or further decreasing the albedo can alter this and make one of the polar caps unstable.

Previous observations from the 1960s and 1970s suggest a more humid southern hemisphere during southern summer (up to 60 pr. μm) compared to more modern observations. Although these data have high uncertainty, if indeed real, our results suggest that exposing water ice to the atmosphere by losing the South Polar Cap perennial CO_2 cover, may explain these observations.

Data Availability Statement

The code for the Mars PCM used for the simulations described in the text can be obtained at http://svn.lmd.jussieu.fr/Planeto/trunk, and a detailed description of it can be found in the User Manual at the following URL: https://web.lmd.jussieu.fr/~lmdz/planets/mars/user_manual.pdf. An example of the start and configuration files can be found at Vos, Aharonson, Schörghofer, Forget, Lange, and Millour (2023), Vos, Aharonson, Schörghofer, Forget, and Millour (2023). No other data set was used in this work.

Acknowledgments

We wish to acknowledge support from the Helen Kimmel Center for Planetary Science, the Minerva Center for Life Under Extreme Planetary Conditions 13599, and the ISF Grant 891/22. This project has received funding from the European Research Council (ERC) under the European Union's Horizon 2020 research and innovation program (Grant 835275, project "Mars Through Time"). The authors wish to thank Misha Kreslavsky for early discussions that led to this research, Lucas Lange for the useful comments, Joseph Naar for improving the cloud microphysics, and Ehouarn Millour for the help with the PCM. The authors thank Peter Buhler and an anonymous reviewer for the helpful comments that improved the manuscript.

References

Alsaeed, N. R., & Hayne, P. O. (2022). Transport of water into the polar regions of Mars through scavenging by CO_2 snowfall. *Journal of Geophysical Research: Planets*, *127*(11), e2022JE007386. https://doi.org/10.1029/2022JE007386

Bonev, B. P., Hansen, G. B., Glenar, D. A., James, P. B., & Bjorkman, J. E. (2008). Albedo models for the residual south polar cap on Mars: Implications for the stability of the cap under near-perihelion global dust storm conditions. *Planetary and Space Science*, *56*(2), 181–193. https://doi.org/10.1016/j.pss.2007.08.003

Bramson, A. M., Byrne, S., Bapst, J., Smith, I. B., & McClintock, T. (2019). A migration model for the polar spiral troughs of Mars. *Journal of Geophysical Research: Planets*, *124*(4), 1020–1043. https://doi.org/10.1029/2018JE005806

Buhler, P., Ingersoll, A., Piqueux, S., Ehlmann, B. L., & Hayne, P. O. (2020). Coevolution of Mars's atmosphere and massive south polar CO_2 ice deposit. *Nature Astronomy*, *4*(4), 364–371. https://doi.org/10.1038/s41550-019-0976-8

Buhler, P. B., Ingersoll, A. P., Ehlmann, B. L., Fassett, C. I., & Head, J. W. (2017). How the Martian residual south polar cap develops quasi-circular and heart-shaped pits, troughs, and moats. *Icarus*, *286*, 69–93. https://doi.org/10.1016/j.icarus.2017.01.012

Buhler, P. B., & Piqueux, S. (2021). Obliquity-driven CO_2 exchange between Mars' atmosphere, regolith, and polar cap. *Journal of Geophysical Research: Planets*, *126*(5), e2020JE006759. https://doi.org/10.1029/2020JE006759

Byrne, S. (2009). The polar deposits of Mars. *Annual Review of Earth and Planetary Sciences*, *37*(1), 535–560. https://doi.org/10.1146/annurev.earth.031208.100101

Byrne, S., Zuber, M., & Neumann, G. (2008). Interannual and seasonal behavior of Martian residual ice-cap albedo. *Planetary and Space Science*, *56*(2), 194–211. https://doi.org/10.1016/j.pss.2006.03.018

Dundas, C. M., Mellon, M. T., Posiolova, L. V., Miljković, K., Collins, G. S., Tornabene, L. L., et al. (2023). A large new crater exposes the limits of water ice on Mars. *Geophysical Research Letters*, *50*(2), e2022GL100747. https://doi.org/10.1029/2022GL100747

Emmett, J., Murphy, J., & Kahre, M. (2020). Obliquity dependence of the formation of the Martian polar layered deposits. *Planetary and Space Science*, *193*(105047), 105047. https://doi.org/10.1016/j.pss.2020.105047

Fedorova, A., Trokhimovsky, S., Korablev, O., & Montmessin, F. (2010). Viking observation of water vapor on Mars: Revision from up-to-date spectroscopy and atmospheric models. *Icarus*, *208*(1), 156–164. https://doi.org/10.1016/j.icarus.2010.01.018

Fenton, L., Geissler, P., & Haberle, R. (2007). Global warming and climate forcing by recent albedo changes on Mars. *Nature*, *446*(7136), 646–649. https://doi.org/10.1038/nature05718

Forget, F., Hourdin, F., Fournier, R., Hourdin, C., Talagrand, O., Collins, M., et al. (1999). Improved general circulation models of the Martian atmosphere from the surface to above 80 km. *Journal of Geophysical Research*, *104*(E10), 24155–24175. https://doi.org/10.1029/1999JE001025

Forget, F., Millour, E., Madeleine, J.-B., Colaitis, A., Spiga, A., Montabone, L., et al. (2011). *Back to the basics: Improving the prediction of temperature, pressure and winds in the LMD general circulation model*. Fourth International Workshop on the Mars Atmosphere.

Haberle, R. M., & Jakosky, B. M. (1990). Sublimation and transport of water from the north residual polar cap on Mars. *Journal of Geophysical Research*, *95*(B2), 1423–1437. https://doi.org/10.1029/JB095iB02p01423

Innanen, A. C., Landis, M. E., Hayne, P. O., & Moores, J. E. (2022). Possible atmospheric water vapor contribution from Martian Swiss cheese terrain. *The Planetary Science Journal*, *3*(10), 242. https://doi.org/10.3847/psj/ac979e

Jakosky, B. M., & Barker, E. S. (1984). Comparison of ground-based and Viking orbiter measurements of Martian water vapor: Variability of the seasonal cycle. *Icarus*, *57*(3), 322–334. https://doi.org/10.1016/0019-1035(84)90121-0

Lange, L., Forget, F., Banfield, D., Wolff, M., Spiga, A., Millour, E., et al. (2022). Insight pressure data recalibration, and its application to the study of long-term pressure changes on Mars. *Journal of Geophysical Research: Planets*, *127*(5), e2022JE007190. https://doi.org/10.1029/2022JE007190

Levrard, B., Forget, F., Montmessin, F., & Laskar, J. (2007). Recent formation and evolution of northern Martian polar layered deposits as inferred from a global climate model. *Journal of Geophysical Research*, *112*(E6). https://doi.org/10.1029/2006JE002772

Madeleine, J.-B., Forget, F., Head, J. W., Levrard, B., Montmessin, F., & Millour, E. (2009). Amazonian northern mid-latitude glaciation on Mars: A proposed climate scenario. *Icarus*, *203*(2), 390–405. https://doi.org/10.1016/j.icarus.2009.04.037

Madeleine, J.-B., Forget, F., Millour, E., Montabone, L., & Wolff, M. J. (2011). Revisiting the radiative impact of dust on Mars using the LMD global climate model. *Journal of Geophysical Research*, *116*(E11), E11010. https://doi.org/10.1029/2011JE003855

Madeleine, J.-B., Forget, F., Millour, E., Navarro, T., & Spiga, A. (2012). The influence of radiatively active water ice clouds on the Martian climate. *Geophysical Research Letters*, *39*(23). https://doi.org/10.1029/2012GL053564

Madeleine, J.-B., Head, J. W., Forget, F., Navarro, T., Millour, E., Spiga, A., et al. (2014). Recent ice ages on Mars: The role of radiatively active clouds and cloud microphysics. *Geophysical Research Letters*, *41*(14), 4873–4879. https://doi.org/10.1002/2014GL059861

Malin, M. C., Caplinger, M. A., & Davis, S. D. (2001). Observational evidence for an active surface reservoir of solid carbon dioxide on Mars. *Science*, *294*(5549), 2146–2148. https://doi.org/10.1126/science.1066416

Mellon, M. T., Arvidson, R. E., Sizemore, H. G., Searls, M. L., Blaney, D. L., Cull, S., et al. (2009). Ground ice at the Phoenix landing site: Stability state and origin. *Journal of Geophysical Research*, *114*(E1). https://doi.org/10.1029/2009JE003417

Millour, E., Forget, F., Spiga, A., Vals, M., Zakharov, V., Montabone, L., & MCD Development Team. (2018). The Mars climate database (version 5.3). In *From Mars express to exomars* (p. 68).

Montabone, L., Forget, F., Millour, E., Wilson, R., Lewis, S., Cantor, B., et al. (2015). Eight-year climatology of dust optical depth on Mars. *Icarus*, *251*, 65–95. https://doi.org/10.1016/j.icarus.2014.12.034

Montmessin, F., Haberle, R. M., Forget, F., Langevin, Y., Clancy, R. T., & Bibring, J.-P. (2007). On the origin of perennial water ice at the south pole of Mars: A precession-controlled mechanism? *Journal of Geophysical Research*, *112*(E8). https://doi.org/10.1029/2007JE002902

Morgan, G. A., Putzig, N. E., Perry, M. R., Sizemore, H. G., Bramson, A. M., Petersen, E. I., et al. (2021). Availability of subsurface water-ice resources in the northern mid-latitudes of Mars. *Nature Astronomy*, *5*(3), 230–236. https://doi.org/10.1038/s41550-020-01290-z

Navarro, T., Madeleine, J.-B., Forget, F., Spiga, A., Millour, E., Montmessin, F., & Määttänen, A. (2014). Global climate modeling of the Martian water cycle with improved microphysics and radiatively active water ice clouds. *Journal of Geophysical Research: Planets*, *119*(7), 1479–1495. https://doi.org/10.1002/2013JE004550

Phillips, R. J., Davis, B. J., Tanaka, K. L., Byrne, S., Mellon, M. T., Putzig, N. E., et al. (2011). Massive CO_2 ice deposits sequestered in the south polar layered deposits of Mars. *Science*, *332*(6031), 838–841. https://doi.org/10.1126/science.1203091

Piqueux, S., & Christensen, P. R. (2008). Deposition of CO_2 and erosion of the Martian south perennial cap between 1972 and 2004: Implications for current climate change. *Journal of Geophysical Research*, *113*(E2). https://doi.org/10.1029/2007JE002969

Plaut, J. J., Picardi, G., Safaeinili, A., Ivanov, A. B., Milkovich, S. M., Cicchetti, A., et al. (2007). Subsurface radar sounding of the south polar layered deposits of Mars. *Science*, *316*(5821), 92–95. https://doi.org/10.1126/science.1139672

Putzig, N. E., Mellon, M. T., Kretke, K. A., & Arvidson, R. E. (2005). Global thermal inertia and surface properties of Mars from the MGS mapping mission. *Icarus*, *173*(2), 325–341. https://doi.org/10.1016/j.icarus.2004.08.017

Smith, M. D. (2004). Interannual variability in TES atmospheric observations of Mars during 1999–2003. *Icarus*, *167*(1), 148–165. https://doi.org/10.1016/j.icarus.2003.09.010

Smith, P. H., Tamppari, L. K., Arvidson, R. E., Bass, D., Blaney, D., Boynton, W. V., et al. (2009). H_2O at the Phoenix landing site. *Science*, *325*(5936), 58–61. https://doi.org/10.1126/science.1172339

Thomas, P., Calvin, W., Cantor, B., Haberle, R., James, P., & Lee, S. (2016). Mass balance of Mars' residual south polar cap from CTX images and other data. *Icarus*, *268*, 118–130. https://doi.org/10.1016/j.icarus.2015.12.038

Thomas, P., Calvin, W., & James, P. (2020). Debris accumulations of CO_2 ice in the south polar residual cap of Mars: Longevity and processes. *Icarus*, *341*, 113625. https://doi.org/10.1016/j.icarus.2020.113625

Thomas, P., Malin, M., James, P., Cantor, B., Williams, R., & Gierasch, P. (2005). South polar residual cap of Mars: Features, stratigraphy, and changes. *Icarus*, *174*(2), 535–559. https://doi.org/10.1016/j.icarus.2004.07.028

Van Hemelrijck, E. (1983). The effect of orbital element variations on the mean seasonal daily insolation on Mars. *The Moon and the Planets*, *28*(2), 125–136. https://doi.org/10.1007/BF00927853

Vincendon, M., Audouard, J., Altieri, F., & Ody, A. (2015). Mars express measurements of surface albedo changes over 2004–2010. *Icarus*, *251*, 145–163. https://doi.org/10.1016/j.icarus.2014.10.029

Vos, E., Aharonson, O., & Schorghofer, N. (2019). Dynamic and isotopic evolution of ice reservoirs on Mars. *Icarus*, *324*, 1–7. https://doi.org/10.1016/j.icarus.2019.01.018

Vos, E., Aharonson, O., Schörghofer, N., Forget, F., Lange, L., & Millour, E. (2023). Paleo-evolution of martian subsurface ice and its role in the polar physical and isotopic layering [Dataset]. *Zenodo*, *128*(10). https://doi.org/10.5281/zenodo.8173921

Vos, E., Aharonson, O., Schörghofer, N., Forget, F., & Millour, E. (2023). Paleo-evolution of Martian subsurface ice and its role in the polar physical and isotopic layering. *Journal of Geophysical Research: Planets*, *128*(10), e2023JE007822. https://doi.org/10.1029/2023JE007822
Vos, E., Aharonson, O., Schörghofer, N., Forget, F., Millour, E., Rossi, L., et al. (2022). Stratigraphic and isotopic evolution of the Martian polar caps from paleo-climate models. *Journal of Geophysical Research: Planets*, *127*(3), e2021JE007115. https://doi.org/10.1029/2021JE007115
Zuber, M. T., Smith, D. E., Solomon, S. C., Abshire, J. B., Afzal, R. S., Aharonson, O., et al. (1998). Observations of the north polar region of Mars from the Mars orbiter laser altimeter. *Science*, *282*(5396), 2053–2060. https://doi.org/10.1126/science.282.5396.2053